In vitro observation of dynamic ordering processes in the extracellular matrix of living, adherent cells

Mark-Oliver Diesner
Department for Molecular Evolution and Genomics, Center for Organismal Studies, University of Heidelberg, D-69120 Heidelberg, Germany and Institute of Toxicology and Genetics, Karlsruhe Institute of Technology, D-76344 Eggenstein-Leopoldshafen, Germany

Alexander Welle and Murat Kazanci
Institute for Biological Interfaces I, Karlsruhe Institute of Technology, D-76344 Eggenstein-Leopoldshafen, Germany

Peter Kaiser and Joachim Spatz
Department of New Materials and Biosystems, Max Planck Institute for Intelligent Systems and Department Biophysical Chemistry, University of Heidelberg, Heisenbergstr. 3, 70569 Stuttgart, Germany

Patrick Koelsch[a)]
Department of Applied Physical Chemistry, University of Heidelberg, D-69120 Heidelberg, Germany and Institute of Toxicology and Genetics, Karlsruhe Institute of Technology, D-76344 Eggenstein-Leopoldshafen, Germany

(Received 11 August 2011; accepted 23 September 2011; published 17 October 2011)

Collecting information at the interface between living cells and artificial substrates is exceedingly difficult. The extracellular matrix (ECM) mediates all cell–substrate interactions, and its ordered, fibrillar constituents are organized with nanometer precision. The proceedings at this interface are highly dynamic and delicate. In order to understand factors governing biocompatibility or its counterpart antifouling, it is necessary to probe this interface without disrupting labels or fixation and with sufficient temporal resolution. Here the authors combine nonlinear optical spectroscopy (sum-frequency-generation) and microscopy (second-harmonic-generation), fluorescence microscopy, and quartz crystal microgravimetry with dissipation monitoring in a strategy to elucidate molecular ordering processes in the ECM of living cells. Artificially (fibronectin and collagen I) and naturally ordered ECM fibrils (zebrafish, *Danio rerio*) were subjected to nonlinear optical analysis and were found to be clearly distinguishable from the background signals of diffusive proteins in the ECM. The initial steps of fibril deposition and ordering were observed *in vitro* as early as 1 h after cell seeding. The ability to follow the first steps of cell–substrate interactions in spite of the low amount of material present at this interface is expected to prove useful for the assessment of biomedical and environmental interfaces. © *2011 American Vacuum Society*. [DOI: 10.1116/1.3651142]

I. INTRODUCTION

The biocompatibility of an artificial substrate with an adherent cell type is determined by the interaction of the first cellular layer attaching directly to the substrate and its modifications.[1–4] This interaction takes place in the boundary region between cell and substrate in which the cell deposits extracellular matrix (ECM).[5–8] The composition of this protein film is extremely particular to the cells depositing it. It mirrors not only the adhering cell's type, differentiation, cell cycle progression, and pathological processes but also the affinity of the cells to the substrate on which the adhesion takes place.[9,10]

The ECM consists of small, diffusive proteins and signaling peptides, as well as comparably large fibrillar structures formed by the cells in a dynamic process of deposition, cleavage, mechanical stress, and further deposition.[11–13] These fibrils are typically composed of fibronectin (FN), collagens, fibrillin, laminin, and other substances. In the initial adhesion process, threadlike structures start out with diameters of 5 to 10 nm, reflecting the diameter of individual FN dimers, as shown by transmission electron microscopy.[14,15] These structures are soluble in deoxycholate (DOC) and are usually formed within 1 to 2 h after seeding if cell-cell contact is made.[14] With the aid of transmembrane receptors, the rearrangement of FN into the insoluble and stable fibrillar state begins after 2 to 4 h and progresses through the next 30 h.[16,17] The detection of FN fibrils using fluorescence microscopy either takes several days, over which cells are allowed to grow to confluency and the fibril deposition and maturation progresses enough to make them detectable,[18–20] or can be achieved after an hour if cells are seeded to confluency and large amounts of prelabeled plasma FN are added.[12,21]

A general challenge encountered when using fluorescent probes on interfacial ECM is the low amount of material, which makes the discrimination between fibrils in the cell-cell and cell-substrate interactions tedious. This is particularly true in early stages of cell adhesion. However, the initial cell-substrate interaction is crucial when evaluating new coatings for biomedical devices or when aiming to prevent biofouling. Especially in the first hours of cell-surface contact, the bulk of these ordered structures are exceptionally difficult

[a)]Electronic mail: patrick.koelsch@kit.edu

to detect or are below the resolution limit of conventional optical microscopy.[14] Labeling and/or fixating fibrils without affecting the dynamics on the nanometer scale is currently impossible. Another challenge is to assess the amount of fibrillar (e.g., ordered) protein compared to the reservoir of unordered building blocks. ECM proteins that are capable of forming ordered structures are most effective in regulating biological responses when in fibrillar form.[22] In that state they expose otherwise cryptic binding sites that orchestrate ligand binding, further fibril formation, and thus the cellular response to mechanical and chemical cues from the environment.[23] Staining with antibodies is usually not specific to the fibrillation status; that is, whether FN proteins are already assembled into fibrils or merely on standby often remains subjective.

In comparison, the label-free nonlinear optical imaging technique of second-harmonic-generation (SHG) microscopy is exclusively sensitive to ordered structures and has been applied to tissue sections[24–28] or reconstituted ECM matrices.[21,28] However, the SHG microscopy signal of a single cellular layer is limited by the signal-to-noise ratio within an imaging setup. In this study we used sum-frequency-generation (SFG) spectroscopy to detect the onset and development of fibril formation in the ECM at the substrate–cell interface. To the best of our knowledge, we were able to achieve this label-free for the first time, through living cells and as early as 1 h after cell seeding.

SFG spectroscopy has proven well suited for probing various interfaces.[29–40] In particular, this technique has been applied to the *in situ* investigation of biomolecules, including peptides,[41–52] proteins,[53–74] and DNA.[75–79] Previous work from our lab has demonstrated the ability of SFG spectroscopy to detect substrate modifications through a layer of adherent, fixed cells[80] and through living, nonadherent cells.[81] Figure 1 summarizes the experiments with nonadherent cells. Figure 1(a) shows a layer of living erythrocytes (ECs). Figure 1(b) shows our measurement setup, which consisted of a reflective substrate, living cells in their media, and an IR-transparent prism through which the pulsed lasers and the SFG signal are directed.[40] Figure 1(c) shows the normalized SFG spectra using undeuterated and deuterated dodecanethiol (DDT and *d*DDT, respectively) self-assembled monolayers (SAMs) on Au-coated Si wafers. Although the ECs contain the majority of ordered biological structures generally present in cells, they contribute very little to the SFG spectra of alkanethiols.[81] Similar results were reported by Bulard *et al.* using bacteria.[82] As adherent cells also do not modify SFG spectra,[80] it can be concluded that ordered intracellular structures (including membranes) do not contribute significantly to SFG signals in this measurement setup.

To approach the time-resolved SFG measurement of the order phenomena in the ECM of adherent cells central to this publication, we analyzed artificially formed FN fibrils on *d*DDT SAMs. FN was chosen as prominent member of the fibril forming group of ECM proteins and appears early upon cellular adhesion. In addition, collagen structures in the fins of zebrafish (*Danio rerio*) and electrospun fibers of collagen

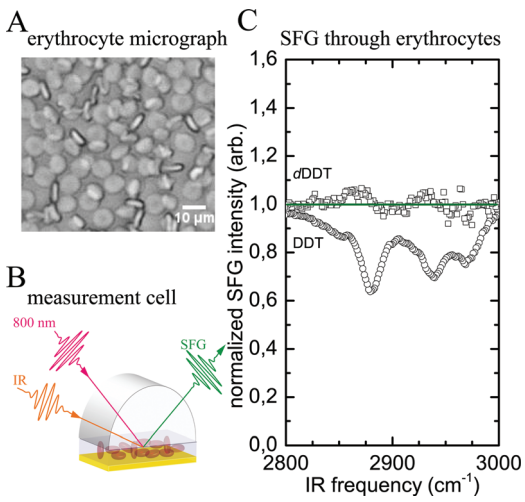

FIG. 1. (Color) (a) Micrograph of a freshly prepared layer of ECs. (b) Schematic depiction of the SFG measurement setup used. (c) SFG signals in the CH region measured through ECs for a *d*DDT SAM (squares) and a DDT SAM (circles) on Au. Data were taken from Ref. 81 and normalized to the nonresonant background contribution. Divergence from 1 (green line) reflects resonant SFG signals.

I (Col I) were investigated using SHG microscopy; Col I was also studied with SFG spectroscopy. In order to mimic smaller, nonstructure forming proteins and their contribution to the SFG signal in comparison to fibrillar structures, bovine serum albumin (BSA) was studied. Finally, ordering phenomena within the ECM were investigated within the first 6 h of adhesion of living fibroblasts to an artificial substrate.

II. MATERIALS AND METHODS

A. Artificial FN fibrils

Polydimethysiloxane (PDMS) pillar arrays, FN, and nanofibrils were prepared in accordance with previously published methods.[83] The micropillar geometry of the PDMS stamps used here had a diameter of 10 μm, and the pillars where spaced at 20 μm from pillar center to pillar center. The FN solution concentration was 100 μg/ml in phosphate-buffered saline (PBS), and the retraction speed of the PDMS stamp against a drop of the protein solution was set to 50 mm/min. Fibrils were then stamped on substrates of 100 nm thick Au films on Si wafers with a 5 nm connective Ti layer.

B. Collagen fibers

1. Preparation of protein solution

A solution of Col I derived from calf skin (generously donated by the Kensey Nash Corporation, USA) was prepared by dissolving the proteins for 5 to 6 h in 1,1,1,3,3,3-hexafluoro-2-propanol (Sigma & Aldrich, Steinheim, Germany) at room temperature. The concentration of collagen in the solution was 4% w/v.

2. Electrospinning

A 2 ml syringe (Omnifix, B. Braun, Melsungen, Germany) was filled with the collagen solution and connected to a

syringe pump (Harvard Apparatus, Holliston, MA, USA). The solution was pushed into a capillary blunt steel needle (21 gauge, 0.7 mm i.d. × 50 mm length) at a constant speed (between 5 and 10 μl/min). The steel needle was connected to a high voltage source (Spellman High Voltage Electronics, West Sussex, UK). The electric potential is needed to start the spinning process and thus form a jet. The applied voltage was 20 kV. Three steel rings with the same charge were placed at the same height and perpendicular to the needle tip in order to stabilize the jet and direct it downward. Two grounded Cu electrodes were placed 15 cm from the needle tip to collect the fibers. The collector has a special design, described elsewhere,[84] to obtain nanofibers. The Cu electrodes were glued on quartz glass and separated by a Teflon spacer. The fiber length was determined by the spacing of the electrodes (1 to 1.5 cm). The fibers were collected on Au-coated Si wafers with a *d*DDT SAM (CDN-Isotopes, Canada). The Si wafers were sputtercoated with 30 nm of Cr followed by 100 nm of Au. Coated wafers were cleaned by 2 h of UV irradiation followed by rinsing with pure ethanol. SAMs were made via incubation in 2 mM alkanethiol-ethanol solution for at least three days.

3. Naturally assembled collagen fibrils from Danio rerio

Naturally formed collagen fibrils such as those found in the bony rays of the fins of the zebrafish *Danio rerio* were used for comparison. For SHG microscopy, a small part of the caudal fin was cut off and stored in buffer immediately after extraction. No fixation or other treatments were applied.

C. Cell culture, sample handling, and fluorescent staining

Rat embryonic fibroblasts (52 wild type) (REF52*wt*) were cultured at 37 °C in a 5% CO_2 atmosphere in Dulbecco's modified Eagle's medium (D-MEM) (Gibco BRL; catalogue no. 10938-025) supplemented with 1% L-glutamine and 10% fetal bovine serum (FBS). After reaching approximately 80% confluency, the cells were rinsed three times with PBS and then treated with a 2.5% trypsin-ethylenediamine tetra-acetic acid solution for 10 min to ensure the degradation of most of the ECM proteins attached to the cell membrane receptors. Cells were then diluted in 7 ml of complete media and centrifuged for 5 min at 800 rpm at room temperature. The cell pellet was then resuspended in 2 ml of media and passaged 1:10 into culture flasks. Passage numbers never exceeded 15 in order to avoid the differences in FN sequestration from the media usually associated with increasing passage numbers.[17] All steps were performed in a sterile hood using sterile techniques and materials. Cells were seeded on hydrophilic gold coated silica surfaces at a density of 1.5×10^5 cells/cm^2 and under the conditions described above in D-MEM containing 1% L-glutamine and 1% FBS in order to minimize the presence of exogenous FN and other ECM constituents. During the measurements, a CaF_2 half-cylindrical prism was placed on the cells and media as depicted in Fig. 1(b). Details on the custom-built temperature-controlled (37 °C) thin-layer analysis cell can be found elsewhere.[40] Here we used a flattened, half-cylindrical CaF_2 prism designed to allow for simultaneous SFG recording and microscopy surveillance of the measurement spot. A microscopy setup was mounted above the sample area. The cells remained wet and were immediately covered with prewarmed PBS or CO_2-independent media (Gibco BRL, catalogue no. 1805-054, supplemented with 1% L-glutamine). Mouse embryonic fibroblasts (NIH/3t3) were treated identically. Cell cycle synchronization was achieved by 16 h of starvation prior to experimentation. The starvation media contained no FBS or L-glutamine.

Fixation and fluorescent staining were carried out in 30 min intervals after cell seeding on translucent Au-coated glass coverslips. The cells were rinsed with prewarmed PBS three times, fixed in 3.7% paraformaldehyde for 30 min, rinsed again three times in PBS, and blocked with BSA for 10 min, after which the primary antibody against FN (MAB1926, Millipore) was applied at a dilution of 1:50. The samples were then incubated for 60 min, after which the cells were rinsed three more times with PBS. Then the second antibody (Alexa 647 conjugated goat anti-mouse; 1:100), together with phalloidin–tetramethylrhodamine B isothiocyanate (1:250) and 4′,6-diamidino-2-phenylindole (DAPI) (1:1000), was applied, and the samples were incubated for 45 min. After being rinsed in PBS another three times, the cells were stored in PBS and immediately subjected to fluorescence microscopy. The cells were visualized with the DeltaVision system (Applied Precision Inc., Issaquah, WA, USA) on an Olympus IX inverted microscope (Olympus, Hamburg, Germany). For fixation, staining, and subsequent fluorescence microscopy, Au-coated coverslips were glued underneath custom-made Petri dishes that had a 1 cm hole in the bottom. For visualization, a 50 × oil immersion objective was used. The Au-coated glass coverslips were made via vapor deposition using a 100-E TePla (PVA TePla AG Plasma Systems, Germany). With 5 nm Ti and 10 nm Au layers, the coverslips remained translucent for use on the inverted fluorescence microscope.

D. Quartz crystal microbalance measurements

A quartz crystal microbalance with dissipation monitoring (QCM-D) (D300 BiolinScientific/Q-Sense AB, Västra Frölunda, Sweden) was used to quantify the adsorption of albumin on gold. The applied instrument uses the ac output of the damped oscillation at 15, 25, and 35 MHz of an AT-cut quartz crystal with gold electrodes to extract the resonance frequencies and dissipation values.[85] Measurements were performed with an "axial flow chamber" having a 0.05 ml exchange volume, a central inflow toward the crystal surface, and an internal temperature controlled loop of approximately 0.5 ml in volume. The presented data were measured in stopped flow mode at (25 ± 0.02) °C. After equilibrating the sample in PBS, bovine serum albumin solutions (Albumin fraction V, Merck) with albumin concentrations between 50 μg/ml and 4 mg/ml in PBS were flushed into the measurement chamber. After the signals had stabilized, the chamber was flushed again with the

buffer, and frequency and dissipation readings were taken. The observed dissipation values due to the formed adsorbate were generally below 2×10^{-6}, indicating only minute contributions of the viscoelastic effects of the protein layer. Therefore, frequency changes were converted to adsorbate thicknesses according to the model of Sauerbrey.[86] The density of all albumin adsorbates was fixed at 1.15×10^6 g/m^3. Following QCM-D experiments, the albumin-coated sensor crystals were dismounted from the measurement chamber and stored under PBS until the following SFG experiment.

E. Nonlinear optical detection

SFG spectra were recorded using a custom made broadband SFG spectrometer (described elsewhere).[40] In the applied measurement mode, the setup utilizes 100 femtosecond (fs) IR pulses with a repetition rate of 1 kHz. These are overlapped with an etalon-shaped narrow band visible pulse at 800 nm at the sample surface. The resulting SFG signal is dispersed on a grating within a spectrometer and subsequently imaged by a backlight-illuminated CCD camera. All spectra reported here were collected in *ppp* polarization in order of increasing wavelength (SFG, visible, and IR). The 1 kHz repetition rate of the laser system allowed for the recording of SFG spectra with a reasonable signal to noise ratio within less than 10 s for samples without cells. The SFG spectra of films on gold substrates show an intense nonresonant (NR) SFG signal, originating from the electronic interband transitions within the metal, together with a resonant (R) signal emanating from the film of interest. The intensity of the generated SFG signal I_{SFG} is related to the infrared (I_{IR}) and visible (I_{VIS}) intensities by the relation

$$I_{SF} \propto \left|\chi^{(2)}\right|^2 I_{IR} I_{VIS}, \tag{1}$$

where

$$\chi^{(2)} = \chi^{(2)}_{NR} + \chi^{(2)}_{R} = |\chi^{(2)}_{NR}| e^{i\phi_{NR}} + \sum_k \left| \frac{A_k}{(\omega_{IR} - \omega_k) + i\Gamma_k} \right| e^{i\phi_{R,k}}. \tag{2}$$

$\chi_{NR}{}^2$, $\chi_R{}^2$, ϕ_{NR}, $\phi_{R,k}$, A_k, and Γ_k are the nonresonant and resonant contributions to and phases in the second-order surface nonlinear susceptibility and the amplitude and linewidth of the kth surface vibrational mode with frequency ω_k, respectively. All SFG spectra were fitted using Eq. (2) and normalized to the intensity profile of a 100 fs IR pulse by assuming a Gaussian function for the IR intensity with a typical width of around 200 cm^{-1}.

Living cells were measured using SFG spectroscopy at an energy of 3 μJ per pulse for both the IR and the visible beams. These settings ensured the most stable measurement conditions, as the appearance of bubbles at the irradiation site occurred more frequently at higher intensities. Tests for laser-induced damage indicated no significant detrimental effects in living rat embryonic fibroblasts after 30 min under simultaneous irradiation with 20 μJ femtosecond IR pulses (3.3 μm) and 7 μJ picosecond visible pulses (0.8 μm), both with a repetition rate of 1 kHz.[80] Observations of the irradiated samples after 16 h of incubation under standard cell culture conditions indicated cell adhesion and proliferation attributable to a healthy population. The SFG signal was optimized in a cell-free area of the sample, after which the sample stage was adjusted so that the input laser beams would hit a confluent cell layer. The accumulation time under these conditions was 40 s.

The fact that all measurements could be normalized to the nonresonant background of Au made comparisons between different spectra over time possible. The square of the sum of the amplitudes A_k in a given spectral region was used to determine the integrated resonant SFG intensity, and this quantity was used to estimate the amount of ordered structures underneath the cells. The linewidth Γ_k was limited to around 8 cm^{-1} for all fits. In the case of DDT SAMs, the initial peak positions were taken from earlier studies and kept fixed in Eq. (2) to obtain the best fit with the phase $\phi_{R,k}$ as a parameter. For BSA, the initial peak positions were taken from the literature and adjusted during the fitting procedure. This was not possible for FN and cellular studies, in which $\phi_{R,k}$ and ω_k are not known *a priori*. Therefore, we used them as free parameters within the fitting routine, allowing up to ten different ω_k values in order to optimize the fit. This introduces some ambiguity regarding exact numbers; therefore, we focus here only on the sum of the resonant signals. Although we make use of the ability to get vibrational information, similar results may be obtained using SHG spectroscopy.

Samples for SHG imaging were not treated any further. The fragment of *Danio rerio* fin was imaged under a coverslip in PBS with a 40× water immersion objective (HCX APO L U-V-I 40.0 × 0.80 WATER). The microscope for the SHG setup was a Leica TCS SP5 MP CFS with a 430/20 filter for detection.

III. RESULTS

A. Nonlinear susceptibility of artificial FN fibrils

FN appears early in cell adhesion processes and is crucial for further ECM development and the assembly of other fibrillar ECM constituents.[19] Early fibronectin fibrils display amyloid structures, implying an ordered conformation detectable with SFG spectroscopy. The manner of fibril production used here employs forces applied to the globular FN molecule that partially unfold the dimer and open up the possibility for the transmolecular interaction essential for the fibril formation process.[83,87,88] This application of mechanical stress is similar to fibrillogenesis *in vivo*. Figure 2(a) shows a microscopy picture of fluorescently labeled artificial FN fibrils on a Au-coated Si wafer displaying the typical geometric pattern of the stamping technique employed.

The SFG spectrum in the CH-stretching region between 2800 and 3000 cm^{-1} of a similarly prepared sample, but without labeling of FN, is shown is Fig. 2(b). The spectrum was normalized to the nonresonant background of the gold substrate, and divergence from 1 (green line) represents the

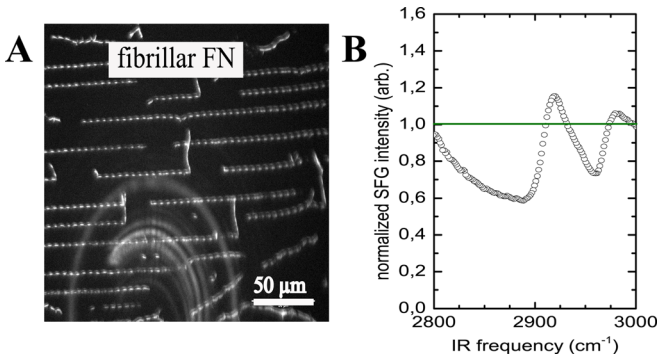

FIG. 2. (Color online) (a) Fibrillar FN on Au-coated substrate; scale bar = 50 μm. (b) Resonant contributions to SFG spectra of fibrillar FN.

resonant contributions of the FN fibrils. The strong resonant contributions, comparable to highly ordered SAMs (Fig. 1), indicate a well-ordered conformation of the FN fibrils. Rotating the same sample and measuring at different positions had little effect on the SFG signal, indicating no preferential horizontal orientation of the probed CH-groups. A spectral comparison between fluorescently labeled (not shown) and unlabeled FN gave similar results, indicating that the presence of labels had little to no effect on SFG signals. A slight contribution of siloxane oligomers was detected in the SFG spectra of control samples without FN fibrils. This signal was used as a background for the calculation of the signal intensity detected from FN fibrils.

The observation of a strong SFG signal for the fibrils studied here holds great promise for the detection of naturally assembled fibrils from living cells. Unfortunately there is no way of obtaining structurally unmodified FN fibrils from natural sources. Usually FN fibrils are closely interlinked with other ECM constituents and cannot be readily isolated without changing their secondary structure significantly. This is, however, possible for other fibrillar ECM constituents such as collagen, e.g., from ligaments or cartilage.

B. Fibrillar appearance does not necessarily come with molecular order

Col I is another abundant fibril-forming ECM protein. The timepoint of fibril appearance and the fibrils' composition is cell type dependant and closely linked to the pre-existence of FN fibrils. SHG and SFG signals from natural Col I fibrils have been extensively discussed in the literature.[24–28,68] Naturally formed Col I fibrils display a high degree of second order nonlinear susceptibility, as can be seen in Fig. 3(a). The SHG microscopy picture shown here is from an excision of the caudal fin of a zebrafish (*Danio rerio*). The rays of the fin are composed of highly aligned Col I fibrils that are partially mineralized with hydroxyapatite in amorphous and crystalline form to form bony rays.[89–91] As can be seen in the figure, only the individual Col I fibrils are visible, indicating that the centrosymmetric hexagonal crystal lattice of hydroxyapatite yields no detectable SHG response.

Nonetheless, the macroscopic fibrillar appearance is not in itself sufficient to lead to a conclusion of molecular order. This is of particular importance when fabricating biointerfaces industrially. Col I is often used for the purpose of making artificial substrates. If the fibrils are fabricated in the laboratory rather than harvested from cell cultures, a frequently employed method is electrospinning. It yields controllable and reproducible fibrils, as can be seen in Figs. 3(b) and 3(c), which show a brightfield image of electrospun collagen threads and a confocal image showing the characteristic autofluorescence of collagen, respectively. Figures 3(d) and 3(e) show the SHG picture of the same fibrils and the

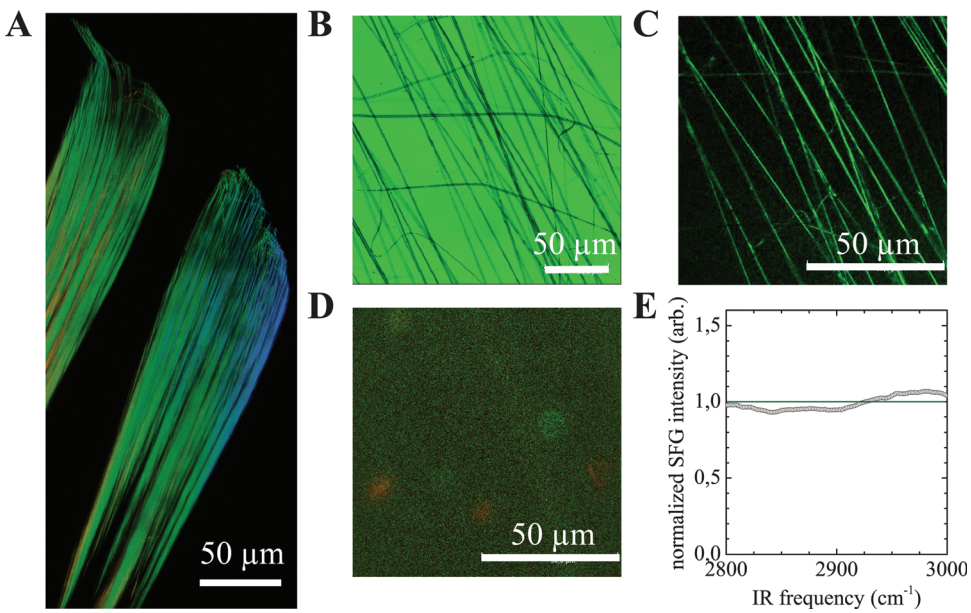

FIG. 3. (Color) (a) SHG picture of natural collagen fibrils found in zebrafish (*Danio rerio*) caudal fin rays (color coding reflects the depth of the z-stack). (b) Brightfield image of electrospun collagen fibrils. (c) Col I autofluorescence of the same spot as in (b) with a slightly higher magnification. (d) SHG image of the area shown in (b) and (c); normalized SFG spectrum of electrospun Col I fibrils.

corresponding SFG spectrum, respectively. No signals can be detected with either method, indicating the lack of order in spite of the fibril-like appearance and higher amount of fibrillar material as compared to the artificial FN fibrils. This example demonstrates the usefulness of identifying order when comparing natural and artificial structures.

C. Signal contributions from ordered protein adsorbates on the cell culture substrate

The adhesion of cells on any man-made cell culture substrate is preceded by a rapid and largely irreversible adsorption of proteins from serum containing cell culture media. This leads to a layer that potentially interferes with the SFG and SHG detection of ECM components. Here we investigate SFG spectra obtained from adsorbed BSA in order to quantify the magnitude of the signals from nonstructure forming ECM constituents in comparison to ordered fibrillar structures. BSA ($M_w = 66.5$ kDa) is the most abundant plasma protein; its structure is stabilized by 17 disulfide bonds, and it forms monolayers on substrates.[92]

Figure 4(a) shows the normalized SFG spectra in the CH stretching region obtained from BSA adsorbates on gold from BSA solutions in PBS from 50 μg/ml to 4 mg/ml. In order to quantify the SFG signal intensities, the sum of the amplitudes A_k obtained by fitting the spectra shown in Fig. 4(a) are plotted as a function of the bulk concentration in Fig. 4(b). The integrated intensity of adsorbed albumin levels off into a plateau at 1 mg/ml, at which point the surface mass detected by QCM-D remains constant at about 700 ng/cm^2 [Fig. 4(c)]. This is most likely due to steric constraints that prohibit protein reorientation at the surface or partial denaturation as observed by Kim and Somorjai.[93] The SFG signal intensity for the FN fibrils discussed in Fig. 2 is also shown here as a dashed blue line for comparison.

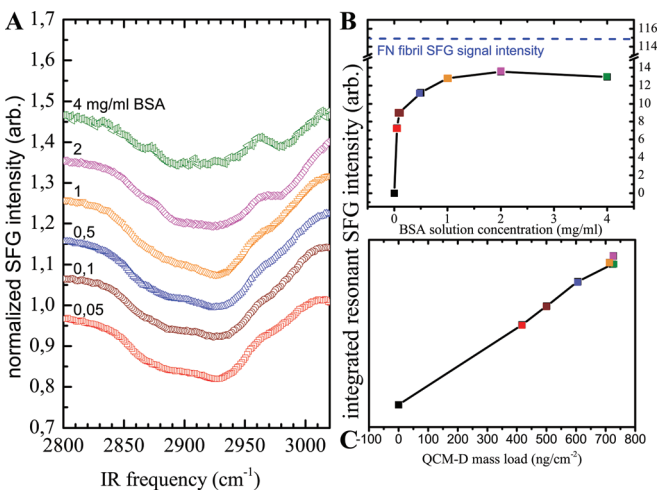

FIG. 4. (Color) Study of BSA as a model protein for assessing the signal intensities of nonordered small proteins at hydrophilic interfaces in comparison to those of unordered FN. (a) Resonant SFG contributions from surfaces coated with BSA at different solution concentrations in the CH region. Color coding for all plots refers to the concentration of BSA in the coating solution. (b) Integrated SFG signal intensity as a function of BSA solution concentration. The blue line depicts the integrated signal intensity of FN fibrils from Fig. 2(b). Note the *y*-axis break between the BSA and FN signals. (c) SFG signal intensity vs surface mass load of BSA as determined by QCM-D experiments.

As shown in Fig. 4(c), it was observed via QCM-D that the reached BSA areal mass loads obtained for sufficiently long adsorption times are concentration dependant. We attribute this behavior to the adsorption, with a kinetic dependent on the solution concentration of the protein coupled with surface induced unfolding. The kinetic of protein denaturation is independent of the solution concentration, similar to results obtained from fibrinogen adsorption studies.[94] The fast adsorption of intact proteins in the high concentration regime leads to a fast occupation of many available surface sites by randomly oriented molecules. In contrast, low protein concentrations in the solution slow down the adsorption and thereby increase the possibility of denaturation. Under these conditions, proteins unfold to maximize protein–substrate interactions, leading to increased contact areas and a reduced mass of the adsorbate. In parallel, the directed interactions of the substrate with the structures of the adsorbed proteins should result in increased anisotropy of the film.[67,93] Albumin should have a limited number of molecular conformations in comparison to FN (440 kDa) when unfolding on a characteristic substrate. Thus, the obtained SFG activity can be regarded as an upper limit for small, non-structure-forming proteins in the ECM.

In conclusion, it has to be noted that SFG is sensitive enough to discriminate between rather random and well-ordered protein monolayers on a substrate. However, a well-ordered monolayer of albumin does not generate SFG signals as strong as those of FN fibrils, as they are important building blocks of the ECM produced by living cells upon adhesion to a cell culture substrate, as shown in the following *in vitro* SFG experiments.

D. ECM fibril formation over time

The high repetition rate of femtosecond laser systems enables spectral recording within seconds. This allows time-resolved studies of dynamic processes such as the development of ordered structures in the ECM of adherent cells. The applicability of SFG in the detection of ECM fibril formation in a fixed state has already been demonstrated.[80] Here we focus on the dynamic detection of this process over time and *in vitro*.

REF52*wt* cells were seeded on Au-coated Si wafers to near confluency, covering 90% of the surface after adhesion and spreading. The first sample was mounted after 70 min on the SFG sample stage as described above. All time points mentioned are relative to the time of the cell seeding. A steady, low SFG signal was detected from the onset of the measurements (see Fig. 5). After 230 min, the signal intensity began to increase, and it reached a maximum at 280 min. From that point, the signal intensity decreased steadily and reached baseline levels after 6 h. Longer experiments show a total loss of the signal at about 7.5 h. Further measurements for up to 48 h show no reappearance of resonant signals (data not shown).

NIH/3t3 cells yielded similar data (see Fig. 6). The onset of resonant signal increase is at about 280 min, and the

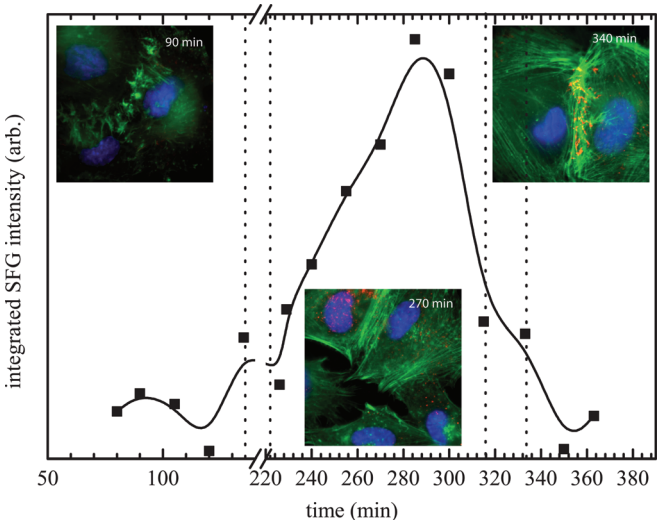

FIG. 5. (Color) Integrated SFG intensity in the CH region over time. Au-coated Si wafers with a confluent layer of REF52*wt* cells adhering to them were exchanged at the time points indicated by the vertical bars. The curved lines are guides for the eye and do not represent a fit of the data shown. Fluorescent micrographs show REF52*wt* cells stained for DNA (DAPI, blue), actin (phalloidin, green) and FN (MAB1926, red). The micrographs were taken at the times indicated on the pictures as part of a 30 min time lapse series.

signal continues to increase until about 380 min. After that point the signal decreases to reach a plateau phase 70 min in length. The resonant signal subsides and vanishes entirely at about 10 h (data not shown). The presence of only a thin film of liquid above the cells necessitates frequent sample changes due to water evaporation of the media. The dotted vertical lines in both graphs indicate sample changes. In order to verify the plateau phase in Fig. 6, replicas were made from 90 to 600 min and exclusively for the time frame of its duration (green line; circles).

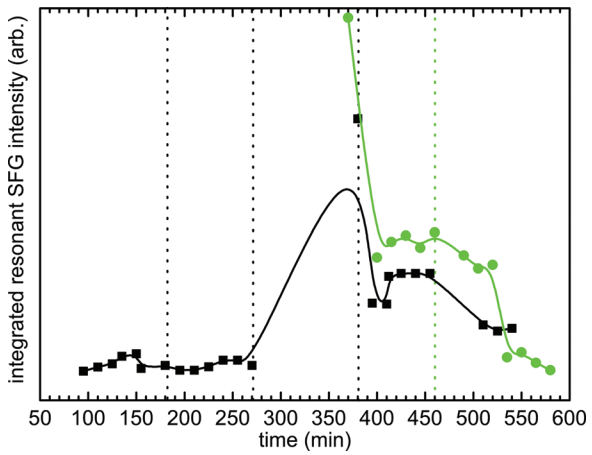

FIG. 6. (Color) Integrated SFG intensity in the CH region over time. Au-coated silicon wafers with a confluent layer of NIH/3t3 cells adhering to them where exchanged as indicated by the vertical bars. An example of the reproducible measurements of the plateau phase observed for this cell type is shown in green. The curved lines are a guide for the eye and do not represent a fit of the data shown.

The data shown in Figs. 5 and 6 are the result of one experimental run. All experiments were reproduced several times, with sample changes at different timepoints resulting in a similar time-dependant development. It should be noted that the observed results are not influenced by the sample changes (green data points in Fig. 6).

Fluorescent microscopy done in parallel to the experiments revealed trace amounts of FN (see Fig. 5). Col I and Col III were not detectable (data not shown). The fluorescent pictures show an increase in FN presence over time. The elongated structures between adjacent cells at 340 min were frequently visible and could indicate fibrillar FN or FN aggregation in preparation for fibril formation. The cell-substrate ECM compartment yielded no FN signal at this stage.

The overall development of ordered structures underneath the two cell types probed here indicates a lag-phase that is dependant on the cell type and, thus, the adhesion and spreading behavior next to protein expression patterns. As both are fibroblast cell lines, they express ECM proteins abundantly. From the onset of the measurements, a low resonant signal is detectable, in accordance with data in the literature on the presence of 5 to 10 nm FN fibrils. A signal increase for both cell types takes place between 4 and 6 h after seeding. Literature values place the onset of FN fibril restructuring from DOC soluble to insoluble fibrils at roughly 2 to 4 h. This coincides well with the data shown here, considering that the cells were kept in media containing only 1% FBS, which amounts to ten times less nutrition than commonly used for fibril formation experiments. Under these conditions, cell attachment, spreading, and ECM deposition are known to be delayed.

The decrease of the resonant signal after it has reached its maximum value should not be identified as a loss of ordered structure in the ECM. Taking into account biological data on the constant increase of ECM fibrillar constituents for days after cell adhesion, it is more likely that the ECM gradually ceases to be an interfacial structure and becomes a bulk media. The appearance of multiple fibrillar layers of different orientations results in a overall more isotropic arrangement, leading to a decreasing SFG signal with a total loss after 7.5 and 10 h, respectively, for each cell type.

IV. CONCLUSION

The data presented here show the applicability of SFG spectroscopy in the elucidation of dynamic biological processes in the ECM between living cells and artificial substrates. For the first time it is possible to follow the onset of fibrillar ordering, dynamically and label free, as early as 4 h after cell seeding. Furthermore, BSA was used to determine the amount of signal that can be expected from small, non-structure-forming proteins alongside FN fibrils. The signal intensity detected here was significantly lower than that obtained from ordered structures of the ECM.

The SFG results of time-lapse experiments on living cells show the presence of ordered structures at the cell–substrate interface as soon as 1 h after cell seeding. After between 4

and 6 h, a large increase in the resonant signal indicates the onset of major ordering processes in the ECM. REF52*wt* were quicker to adhere and spread on the Au substrate. In accordance with this effect, the increase in the SFG signal appeared 50 min earlier after seeding than with NIH/3t3 cells. The timing of the signal increase in both cell types presumably coincides with the loss of solubility of the FN sequestered by cells, as discussed by McKeown-Longo *et al.*[16] and Mann *et al.*[17] in the 20th century. It is speculated that this loss of solubility has to do with the maturation of the FN fibrils and their interaction with other ECM constituents.[19] Said maturation of the fibrils leads to an initial increase in the signal, as observed here. The retardation of the signal appearance is more than likely a function of the 1% FBS cell culture media, as opposed to the 10% FBS media used in the experiments documented in literature. Concomitantly with slower cell adhesion and spreading, the ECM deposition and ordering are slower. The low amount of FBS in the media minimized the presence of diffusive ECM constituents. Therefore, most of the signal detected here and the timelines recorded are exclusively dependant on the ECM material produced and deposited by the cells in response to the substrate they adhere to.

Parallel fluorescence microscopic observations were conducted involving the fixing and staining of cells for FN, Col I, and Col III. Faint traces of FN could be detected, and Col I and Col III could not be detected, at these early timepoints. FN appeared in dots and occasionally in elongated patches, from which fibril formation could not be conclusively derived. Considering that studies on ECM fibril formation are usually conducted on confluent layers of cells that are generally at least 1 day old and supplemented with large amounts of prestained FN, the lack of a fibrillar appearance in the fluorescent microscopic studies observed here is not surprising.

SFG spectroscopy is a promising technique for the analysis of existing and upcoming biological substrates. Currently, peptide fragments are commonly used to trigger biological signaling via artificial substrates. The geometry and orientation of such ligands play an important role in the interaction with the cells.[95] To this end, more complex materials made from artificially ordered ECM constituents are also employed in an attempt to offer cell cultures biological niches as close as possible to their natural environment. Artificial ordered structures made from appropriate biomolecules can be achieved via a number of experimental procedures. Cataloging nonlinear optical signals from ordered biological structures might prove to be a straightforward way to compare artificially generated constructs with their biological counterparts. The results from electrospun Col I fibrils reported here might serve as an example for this procedure. Among the various ways of gaining fibril shaped Col I aggregates, electrospinning is elegant but very dependant on the solvent system employed (unpublished data). The fibrils produced here are not ordered similarly to the ones encountered in the ECM of living cells; although the macroscopic appearance is reminiscent of the archetype, the molecular structure is very different.

ACKNOWLEDGMENTS

The authors thank M. Grunze for his continuous and steady support and stimulating discussions. The fragment of zebrafish dorsal fin was kindly provided by C. Grabherr and Gerald the fish. SHG microscopy was done at the labs of Leica Microsystems in Mannheim with the kind help of O. Levai.

[1] D. G. Castner and B. D. Ratner, Surf. Sci. **500**, 28 (2002).
[2] B. K. Canales, L. Higgins, T. Markowski, L. Anderson, Q. A. Li, and M. Monga, J. Endourol. **23**, 1437 (2009).
[3] B. N. Brown, C. A. Barnes, R. T. Kasick, R. Michel, T. W. Gilbert, D. Beer-Stolz, D. G. Castner, B. D. Ratner, and S. F. Badylak, Biomaterials **31**, 428 (2010).
[4] C. A. Barnes, J. Brison, R. Michel, B. N. Brown, D. G. Castner, S. F. Badylak, and B. D. Ratner, Biomaterials **32**, 137 (2011).
[5] M. J. P. Biggs, R. G. Richards, N. Gadegaard, C. D. W. Wilkinson, and M. J. Dalby, J. Orthop. Res. **25**, 273 (2007).
[6] M. J. P. Biggs, R. G. Richards, and M. J. Dalby, Nanomedicine **6**, 619 (2010).
[7] E. Lamers, X. F. Walboomers, M. Domanski, J. te Riet, F. C. M. J. M. van Delft, R. Luttge, L. A. J. A. Winnubst, H. J. G. E. Gardeniers, and J. A. Jansen, Biomaterials **31**, 3307 (2010).
[8] K. von der Mark, J. Park, S. Bauer, and P. Schmuki, Cell Tissue Res. **339**, 131 (2010).
[9] C. T. Brighton, J. R. Fisher, S. E. Levine, J. R. Corsetti, T. Reilly, A. S. Landsman, J. L. Williams, and L. E. Thibault, J. Bone Jt. Surg., Am. Vol. **78**, 1337 (1996).
[10] P. F. Davies, K. A. Barbee, M. V. Volin, A. Robotewskyj, J. Chen, L. Joseph, M. L. Griem, M. N. Wernick, E. Jacobs, D. C. Polacek, N. DePaola, and A. I. Barakat, Annu. Rev. Physiol. **59**, 527 (1997).
[11] C. Zhong, M. Chrzanowska-Wodnicka, J. Brown, A. Shaub, A. M. Belkin, and K. Burridge, J. Cell Biol. **141**, 539 (1998).
[12] I. Wierzbicka-Patynowski and J. E. Schwarzbauer, J. Cell Sci. **116**, 3269 (2003).
[13] Y. Mao and J. E. Schwarzbauer, Matrix Biol. **24**, 389 (2005).
[14] L. B. Chen, A. Murray, R. A. Segal, A. Bushnell, and M. L. Walsh, Cell **14**, 377 (1978).
[15] J. Engel, E. Odermatt, A. Engel, J. A. Madri, H. Furthmayr, H. Rohde, and R. Timpl, J. Mol. Biol. **150**, 97 (1981).
[16] P. J. McKeown-Longo and D. F. Mosher, J. Cell Biol. **97**, 466 (1983).
[17] D. M. Mann, P. J. McKeown-Longo, and A. J. Millis, J. Biol. Chem. **263**, 2756 (1988).
[18] J. E. Wagenseil and R. P. Mecham, Birth Defects Res. C **81**, 229 (2007).
[19] P. Singh, C. Carraher, and J. E. Schwarzbauer, Annu. Rev. Cell Dev. Biol. **26**, 397 (2010).
[20] H. C. Hsia, M. R. Nair, R. C. Mintz, and S. A. Corbett, Plast. Reconstr. Surg. **127**, 2312 (2011).
[21] E. G. Hayman and E. Ruoslahti, J. Cell Biol. **83**, 255 (1979).
[22] J. Sottile and D. C. Hocking, Mol. Biol. Cell **13**, 3546 (2002).
[23] P. P. Girard, E. A. Cavalcanti-Adam, R. Kemkemer, and J. P. Spatz, Soft Matter **3**, 307 (2007).
[24] R. M. Williams, W. R. Zipfel, and W. W. Webb, Biophys. J. **88**, 1377 (2005).
[25] K. Schenke-Layland, Journal of Biophotonics **1**, 451 (2008).
[26] X. Han, R. M. Burke, M. L. Zettel, P. Tang, and E. B. Brown, Opt. Express **16**, 1846 (2008).
[27] R. Cicchi, S. Sestini, V. De Giorgi, D. Massi, T. Lotti, and F. S. Pavone, Journal of Biophotonics **1**, 62 (2008).
[28] K. R. Levental, H. Yu, L. Kass, J. N. Lakins, M. Egeblad, J. T. Erler, S. F. T. Fong, K. Csiszar, A. Giaccia, W. Weninger, M. Yamauchi, D. L. Gasser, and V. M. Weaver, Cell **139**, 891 (2009).
[29] G. L. Richmond, Chem. Rev. **102**, 2693 (2002).
[30] M. Raschke and Y. Shen, Curr. Opin. Solid State Mater. Sci. **8**, 343 (2004).
[31] M. A. Leich and G. L. Richmond, Faraday Discuss. **129**, 1 (2005).
[32] A. Hopkins, C. McFearin, and G. Richmond, Curr. Opin. Solid State Mater. Sci. **9**, 19 (2005).
[33] S. Gopalakrishnan, D. Liu, H. C. Allen, M. Kuo, and M. J. Shultz, Chem. Rev. **106**, 1155 (2006).
[34] Y. R. Shen and V. Ostroverkhov, Chem. Rev. **106**, 1140 (2006).

[35]A. B. Sugiharto, C. Johnson, H. de Aguiar, L. Alloatti, and S. Roke, Appl. Phys. B **91**, 315 (2008).
[36]H. C. Allen, N. N. Casillas-Ituarte, M. R. Sierra-Hernández, X. Chen, and C. Y. Tang, Phys. Chem. Chem. Phys. **11**, 5538 (2009).
[37]F. M. Geiger, Annu. Rev. Phys. Chem. **60**, 61 (2009).
[38]S. Roke, ChemPhysChem **10**, 1380 (2009).
[39]C. Tian and Y. Shen, Chem. Phys. Lett. **470**, 1 (2009).
[40]D. Verreault, V. Kurz, C. Howell, and P. Koelsch, Rev. Sci. Instrum. **81**, 063111 (2010).
[41]J. Kim, K. C. Chou, and G. A. Somorjai, J. Phys. Chem. B **106**, 9198 (2002).
[42]O. Mermut, D. C. Phillips, R. L. York, K. R. McCrea, R. S. Ward, and G. A. Somorjai, J. Am. Chem. Soc. **128**, 3598 (2006).
[43]X. Chen and Z. Chen, Biochim. Biophys. Acta **1758**, 1257 (2006).
[44]D. Phillips, R. York, O. Mermut, K. McCrea, R. Ward, and G. Somorjai, J. Phys. Chem. C **111**, 255 (2007).
[45]R. York, O. Mermut, D. Phillips, K. McCrea, R. Ward, and G. Somorjai, J. Phys. Chem. C **111**, 8866 (2007).
[46]A. B. Sugiharto, C. M. Johnson, I. E. Dunlop, and S. Roke, J. Phys. Chem. C **221**, 7531 (2008).
[47]R. L. York, G. J. Holinga, D. R. Guyer, K. R. McCrea, R. S. Ward, and G. A. Somorjai, Appl. Spectrosc. **62**, 937 (2008).
[48]T. Weidner, N. F. Breen, G. P. Drobny, and D. G. Castner, J. Phys. Chem. B **113**, 15423 (2009).
[49]R. L. York, G. J. Holinga, and G. A. Somorjai, Langmuir **25**, 9369 (2009).
[50]J. Fick, T. Wolfram, F. Belz, and S. Roke, Langmuir **26**, 1051 (2010).
[51]T. Weidner, N. F. Breen, K. Li, G. P. Drobny, and D. G. Castner, Proc. Natl. Acad. Sci. U.S.A. **107**, 13288 (2010).
[52]G. J. Holinga, R. L. York, R. M. Onorato, C. M. Thompson, N. E. Webb, A. P. Yoon, and G. A. Somorjai, J. Am. Chem. Soc. **133**, 6243 (2011).
[53]J. Kim and P. S. Cremer, ChemPhysChem **2**, 543 (2001).
[54]G. Kim, M. Gurau, J. Kim, and P. S. Cremer, Langmuir **18**, 2807 (2002).
[55]Z. Chen, R. Ward, Y. Tian, F. Malizia, D. H. Gracias, Y. R. Shen, and G. A. Somorjai, J. Biomed. Mater. Res. **62**, 254 (2002).
[56]J. Wang, S. M. Buck, M. A. Even, and Z. Chen, J. Am. Chem. Soc. **124**, 13302 (2002).
[57]J. Wang, S. M. Buck, and Z. Chen, J. Phys. Chem. B **106**, 11666 (2002).
[58]T. S. Koffas, J. Kim, C. C. Lawrence, and G. A. Somorjai, Langmuir **19**, 3563 (2003).
[59]J. Wang, M. L. Clarke, Y. Zhang, X. Chen, and Z. Chen, Langmuir **19**, 7862 (2003).
[60]A. W. Doyle, J. Fick, M. Himmelhaus, W. Eck, I. Graziani, I. Prudovsky, M. Grunze, T. Maciag, and D. J. Neivandt, Langmuir **20**, 8961 (2004).
[61]L. Dreesen, Y. Sartenaer, C. Humbert, A. A. Mani, C. Méthivier, C.-M. Pradier, P. A. Thiry, and A. Peremans, ChemPhysChem **5**, 1719 (2004).
[62]J. Kim, T. S. Koffas, C. C. Lawrence, and G. A. Somorjai, Langmuir **20**, 4640 (2004).
[63]L. Dreesen, C. Humbert, Y. Sartenaer, Y. Caudano, C. Volcke, A. A. Mani, A. Peremans, P. A. Thiry, S. Hanique, and J.-M. Frère, Langmuir **20**, 7201 (2004).
[64]Z. Pászti, J. Wang, M. L. Clarke, and Z. Chen, J. Phys. Chem. B **108**, 7779 (2004).
[65]J. Wang, Z. Paszti, M. A. Even, and Z. Chen, J. Phys. Chem. B **108**, 3625 (2004).
[66]J. Wang, X. Chen, M. L. Clarke, and Z. Chen, Proc. Natl. Acad. Sci. U.S.A. **102**, 4978 (2005).
[67]J. Wang, M. Clarke, X. Chen, M. Even, W. Johnson, and Z. Chen, Surf. Sci. **587**, 1 (2005).
[68]I. Rocha-Mendoza, D. R. Yankelevich, M. Wang, K. M. Reiser, C. W. Frank, and A. Knoesen, Biophys. J. **93**, 4433 (2007).
[69]X. Chen, A. P. Boughton, J. J. G. Tesmer, and Z. Chen, J. Am. Chem. Soc. **129**, 12658 (2007).
[70]J. Wang, S.-H. Lee, and Z. Chen, J. Phys. Chem. B **112**, 2281 (2008).
[71]S. Ye, K. T. Nguyen, S. V. Le Clair, and Z. Chen, J. Struct. Biol. **168**, 61 (2009).
[72]S. Le Clair, K. Nguyen, and Z. Chen, J. Adhes. **85**, 484 (2009).
[73]L. Baugh, T. Weidner, J. E. Baio, P.-C. T. Nguyen, L. J. Gamble, P. S. Stayton, and D. G. Castner, Langmuir **26**, 16434 (2010).
[74]L. Fu, J. Liu, and E. C. Y. Yan, J. Am. Chem. Soc. **133**, 8094 (2011).
[75]Y. Sartenaer, G. Tourillon, L. Dreesen, D. Lis, A. A. Mani, P. A. Thiry, and A. Peremans, Biosens. Bioelectron. **22**, 2179 (2007).
[76]G. Y. Stokes, J. M. Gibbs-Davis, F. C. Boman, B. R. Stepp, A. G. Condie, S. T. Nguyen, and F. M. Geiger, J. Am. Chem. Soc. **129**, 7492 (2007).
[77]H. Asanuma, H. Noguchi, K. Uosaki, and H.-Z. Yu, J. Am. Chem. Soc. **130**, 8016 (2008).
[78]C. Howell, R. Schmidt, V. Kurz, and P. Koelsch, BioInterphases **3**, FC47 (2008).
[79]S. R. Walter and F. M. Geiger, The Journal of Physical Chemistry Letters **1**, 9 (2010).
[80]C. Howell, M.-O. Diesner, M. Grunze, and P. Koelsch, Langmuir **24**, 13819 (2008).
[81]M.-O. Diesner, C. Howell, V. Kurz, D. Verreault, and P. Koelsch, The Journal of Physical Chemistry Letters **1**, 2339 (2010).
[82]E. Bulard, Z. Guo, W. Zheng, H. Dubost, M.-P. Fontaine-Aupart, M. N. Bellon-Fontaine, J.-M. Herry, R. Briandet, and B. Bourguignon, Langmuir **27**, 4928 (2011).
[83]P. Kaiser and J. P. Spatz, Soft Matter **6**, 113 (2010).
[84]L. Buttafoco, N. G. Kolkman, P. Engbers-Buijtenhuijs, A. A. Poot, P. J. Dijkstra, I. Vermes, and J. Feijen, Biomaterials **27**, 724 (2006).
[85]M. Rodahl, F. Höök, C. Fredriksson, C. A. Keller, A. Krozer, P. Brzezinski, M. Voinova, and B. Kasemo, Faraday Discuss. 229 (1997).
[86]G. Sauerbrey, Z. Phys. **155**, 206 (1959).
[87]M. L. Smith, D. Gourdon, W. C. Little, K. E. Kubow, R. A. Eguiluz, S. Luna-Morris, and V. Vogel, PLoS Biol. **5**, e268 (2007).
[88]J. Ulmer, B. Geiger, and J. P. Spatz, Soft Matter **4**, 1998 (2008).
[89]N. C. Bird and P. M. Mabee, Dev. Dyn. **228**, 337 (2003).
[90]K. D. Poss, M. T. Keating, and A. Nechiporuk, Dev. Dyn. **226**, 202 (2003).
[91]J. Mahamid, A. Sharir, L. Addadi, and S. Weiner, Proc. Natl. Acad. Sci. U.S.A. **105**, 12748 (2008).
[92]T. J. Su, R. K. Thomas, Z. F. Cui, and J. Penfold, J. Phys. Chem. B **102**, 8100 (1998).
[93]J. Kim and G. A. Somorjai, J. Am. Chem. Soc. **125**, 3150 (2003).
[94]R. R. Siegel, P. Harder, R. Dahint, M. Grunze, F. Josse, M. Mrksich, and G. M. Whitesides, Anal. Chem. **69**, 3321 (1997).
[95]J. Huang, S. V. Grater, F. Corbellini, S. Rinck, E. Bock, R. Kemkemer, H. Kessler, J. Ding, and J. P. Spatz, Nano Lett. **9**, 1111 (2009).